Report

Cell Reports

Loss of IQSEC3 Disrupts GABAergic Synapse Maintenance and Decreases Somatostatin Expression in the Hippocampus

Graphical Abstract

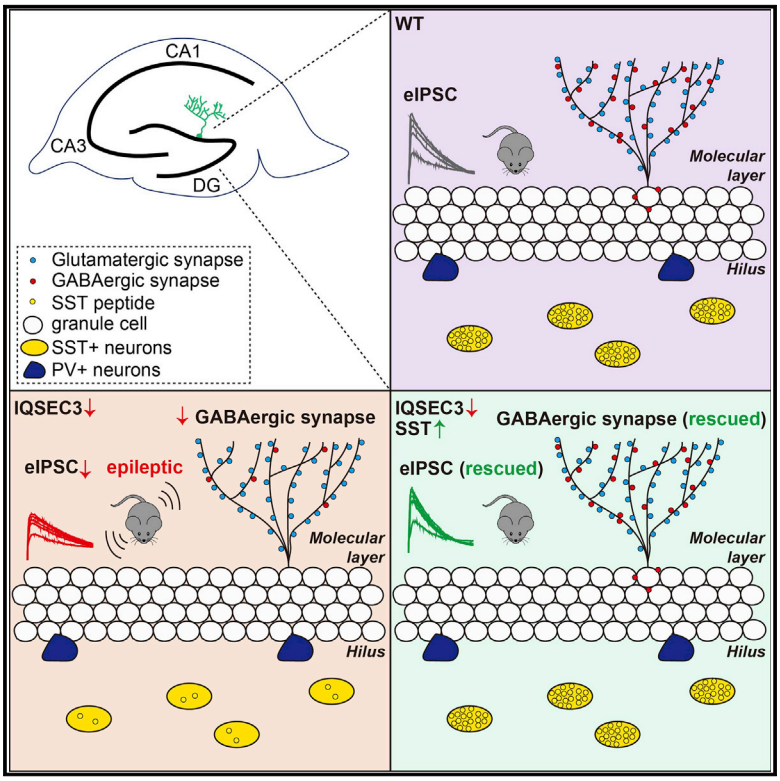

Highlights

- IQSEC3 regulates GABAergic synapse maintenance *in vivo*
- IQSEC3 requires its ARF-GEF activity for its inhibitory action
- IQSEC3 loss decreases SST expression
- SST restores IQSEC3 deficiency-triggered pathologies

Authors

Seungjoon Kim, Hyeonho Kim, Dongseok Park, ..., Eunji Cheong, Jaewon Ko, Ji Won Um

Correspondence

jaewonko@dgist.ac.kr (J.Ko), jiwonum@dgist.ac.kr (J.W.U.)

In Brief

In this study, Kim et al. investigate the effect of loss of function of IQSEC3, a gephyrin-binding GABAergic synapse-specific ARF-GEF, using hippocampal dentate gyrus (DG)-specific IQSEC3-knockdown (KD) mice. Strikingly, IQSEC3 KD causes a massive reduction of somatostatin (SST) expression. The restricted SST expression in SST$^+$ interneurons reverses the pathological phenotypes.

Kim et al., 2020, Cell Reports *30*, 1995–2005
February 11, 2020
https://doi.org/10.1016/j.celrep.2020.01.053

CellPress

Cell Reports
Report

Loss of IQSEC3 Disrupts GABAergic Synapse Maintenance and Decreases Somatostatin Expression in the Hippocampus

Seungjoon Kim,[1,4] Hyeonho Kim,[1,4] Dongseok Park,[1] Jinhu Kim,[1] Joohyeon Hong,[2] Jae Seong Kim,[2] Hyeji Jung,[1] Dongwook Kim,[1] Eunji Cheong,[2] Jaewon Ko,[1,*] and Ji Won Um[1,3,5,*]

[1]Department of Brain and Cognitive Sciences, Daegu Gyeongbuk Institute of Science and Technology (DGIST), 333 Techno Jungangdae-Ro, Hyeonpoong-Eup, Dalseong-Gun, Daegu 42988, Korea

[2]Department of Biotechnology, College of Life Science and Biotechnology, Yonsei University, Seoul 03722, Korea

[3]Core Protein Resources Center, DGIST, 333 Techno Jungangdae-Ro, Hyeonpoong-Eup, Dalseong-Gun, Daegu 42988, Korea

[4]These authors contributed equally

[5]Lead Contact

*Correspondence: jaewonko@dgist.ac.kr (J.Ko), jiwonum@dgist.ac.kr (J.W.U.)

https://doi.org/10.1016/j.celrep.2020.01.053

SUMMARY

Gephyrin interacts with various GABAergic synaptic proteins to organize GABAergic synapse development. Among the multitude of gephyrin-binding proteins is IQSEC3, a recently identified component at GABAergic synapses that acts through its ADP ribosylation factor-guanine nucleotide exchange factor (ARF-GEF) activity to orchestrate GABAergic synapse formation. Here, we show that IQSEC3 knockdown (KD) reduced GABAergic synaptic density *in vivo*, suggesting that IQSEC3 is required for GABAergic synapse maintenance *in vivo*. We further show that IQSEC3 KD in the dentate gyrus (DG) increases seizure susceptibility and triggers selective depletion of somatostatin (SST) peptides in the DG hilus in an ARF-GEP activity-dependent manner. Strikingly, selective introduction of SST into SST interneurons in DG-specific IQSEC3-KD mice reverses GABAergic synaptic deficits. Thus, our data suggest that IQSEC3 is required for linking gephyrin-$GABA_A$ receptor complexes with ARF-dependent pathways to prevent aberrant, runaway excitation and thereby contributes to the integrity of SST interneurons and proper GABAergic synapse maintenance.

INTRODUCTION

Synapses, the basic unit of neural circuits, are fundamental in transferring, processing, and computing neural information in the brain (Südhof, 2017). They are formed at specific sites in neurons and dynamically control and modify their plasticity, a key property that supports essential brain functions. Various classes of synaptic proteins are involved in distinct aspects of synapse formation and serve to coordinate neuronal functions by maintaining a proper balance of the excitation-to-inhibition (E/I) ratio at neural circuits. An imbalanced E/I ratio in multiple brain regions is directly linked to deficits in neural information processing by and between various microcircuits interspersed throughout the brain and is associated with the onset and progression of various brain disorders (Ko et al., 2015; Steinberg et al., 2015). Epilepsy is a prevalent brain disorder characterized by recurrent seizures. Although non-synaptic mechanisms may also be involved, one mechanism that can provoke epileptic seizures is dysregulation of synaptic mechanisms, which induces abnormal organization of neuronal connections and thereby converts a normal neuronal network into a hyperexcitable network (Dudek et al., 1998; Jefferys, 2010). Substantial efforts to develop relevant animal models and rigorous histological studies have contributed to our current understanding of the mechanisms of epileptogenesis, pinpointing key pathological features of various epilepsy types, which include mossy fiber sprouting in the hippocampal dentate gyrus (DG) and loss of various GABAergic interneurons (Leite et al., 2005).

Gephyrin, a master scaffold that interacts with dozens of other GABAergic synaptic components, regulates synapse formation, transmission, and plasticity at GABAergic synapses (Alvarez, 2017; Choii and Ko, 2015; Groeneweg et al., 2018). Multiple copy number variations and single-nucleotide morphisms of gephyrin and its binding proteins collybistin (ARHGEF9) and mammalian target of rapamycin (mTOR) have been strongly implicated in temporal lobe epilepsy (TLE) (Ko et al., 2015). Notably, all TLE-associated gephyrin variants exhibit irregular exon skipping in the N-terminal G-domain (Feng et al., 2010). Consistent with this, knockout mice deficient for these proteins exhibit severe seizures (Ko et al., 2015). In this context, we recently identified a molecular interaction of gephyrin with IQSEC3, a GABAergic synapse-specific guanine nucleotide exchange factor for ADP ribosylation factor (ARF-GEF) (Um, 2017). IQSEC3 promotes GABAergic synapse development in cultured hippocampal neurons in a manner that requires its ARF-GEF activity (Um et al., 2016a). Similar to gephyrin, IQSEC3 downregulation appears to be involved in a subset of neuropsychiatric disorders (Choii and Ko, 2015; Ellis et al., 2016). Moreover, given that molecular components that have been linked to IQSEC3 (i.e., gephyrin, ARHGEF9, and neuroligin-2) are commonly associated with epilepsy and that

IQSEC3 specifically promotes GABAergic synapse development, it is tempting to speculate that IQSEC3 may also be involved in epileptogenesis.

In the present study, we performed extensive analyses to probe whether and how loss of IQSEC3 results in abnormal neuronal network activities that lead to epileptic seizure phenotypes. Knockdown (KD) of IQSEC3 in the hippocampal DG induced a significant decrease in GABAergic synapse density and caused a massive reduction of somatostatin (SST) expression in the DG hilus. Surprisingly, expression of SST in DG-specific IQSEC3-KD mice was sufficient to rescue the IQSEC3 KD-mediated cellular pathologies, an effect that depended on IQSEC3 ARF-GEF activity. Collectively, our results suggest that IQSEC3 ARF activity is essential for maintaining normal GABAergic synapse density and the integrity of SST-positive interneurons (SST^+-INs).

RESULTS

IQSEC3 Is Required for Maintenance of GABAergic Synapse Structure in the DG of Mice

We previously showed that IQSEC3 KD decreases gephyrin puncta size in cultured hippocampal neurons (Um et al., 2016a). However, whether this observation could be recapitulated *in vivo* remained unknown. To probe whether IQSEC3 KD influences structural aspects of GABAergic synapse maintenance, we performed immunohistochemical analyses in mice stereotactically injected in the hippocampal DG with adeno-associated viruses (AAVs) expressing small hairpin RNA (shRNA) targeting *Iqsec3* (sh-IQSEC3) or control shRNA (sh-Control) (Figure 1A; Figure S1). Quantitative immunofluorescence analyses of the GABAergic synaptic markers GAD67 (glutamic acid decarboxylase 67 kDa), VGAT (vesicular GABA transporter) and $GABA_AR\gamma2$ revealed significant decreases in the intensity and density of GAD67, VGAT, and $GABA_AR\gamma2$ puncta in the DG granular cell layer, and the DG hilus and molecular layers, but not in the cortex (a control brain area in which AAVs were not transduced; Figures 1B–1E; Figure S2). In contrast, puncta intensity of VGLUT1 (vesicular glutamate transporter 1), a glutamatergic synaptic marker, was not changed in the DG or cortex (Figure S2). These changes in GAD67, VGAT, and $GABA_AR\gamma2$ intensity and density in the DG of IQSEC3-KD mice were completely rescued by expression of IQSEC3 wild-type (WT) but not an ARF-GEF activity-deficient IQSEC3 E749A mutant (Um et al., 2016a; Figures 1B–1E; see Figure S1C for validation of IQSEC3 E749A by Arf6 activation assay). Collectively, these results demonstrate that the ARF-GEF activity of IQSEC3 is required for the selective regulation of GABAergic synapse formation and maintenance by IQSEC3 *in vivo*.

IQSEC3 Loss Accelerates Seizure Susceptibility in an ARF-GEF Activity-Dependent Manner

We next sought to determine whether IQSEC3 plays a role under epileptogenic conditions, which, like various neurological disorders, are often associated with impaired GABAergic synapse formation and function (Hiester and Santy, 2013; Ko et al., 2015) and a resulting imbalance in E/I ratio at synaptic and circuit levels. Thus, we performed 24 h tethered electroencephalography (EEG) recordings in mice injected into the DG with the indicated AAVs (Figure S3A). Ictal-like EEG discharges, characterized by large amplitudes, long durations (>20 s), and repetitive single or complex spike waveforms, were frequently observed in IQSEC3-KD mice under drug-free conditions; no electrographic signs of spontaneous recurrent seizures were ever detected in control mice (Figures S3B and S3C). These abnormal epileptiform spike patterns were completely rescued by coexpression of IQSEC3 WT but not the IQSEC3 E749A (Figures S3B and S3C). In addition, an analysis of interictal-like epileptiform activity supported the same conclusions (Figures S3D and S3E).

To elucidate in-depth mechanisms underlying IQSEC3-KD-induced epileptic seizures and delineate the effect of IQSEC3 KD on susceptibility to epileptic seizures, we used an acute kainic acid (KA)-induced epileptic mouse model, which has been extensively used to dissect molecular mechanisms underlying initial epileptogenesis event(s) that transforms normal neural networks into hypersynchronous networks (Marriott et al., 2017). Mice injected with the indicated AAVs were intraperitoneally administered KA (15 mg/kg), and their seizure-related behaviors were monitored by video recordings (Figure 2A). The severity of KA-induced convulsive seizures was assessed by scoring responses on a scale from 0 (no abnormal behavior) to 5 (death) using a revised Racine's scale (Racine, 1972; Figures 2B–2F). Average seizure scores for the first 60 min after KA administration were ~1.5-fold higher in IQSEC3-KD mice (3.08 ± 0.15) than in control mice (1.96 ± 0.39) (Figures 2B and 2C). Average seizure scores for the next 60 min were 3.65 ± 0.19 and 2.31 ± 0.16 in IQSEC3-KD and control mice, respectively, indicating that the severity of seizure behaviors persisted in these mice (Figures 2B and 2D). Importantly, the increased seizure susceptibility observed in IQSEC3-KD mice was normalized by coexpression of IQSEC3 WT (2.33 ± 0.19 for first 60 min and 2.65 ± 0.23 for the next 60 mi) but not by coexpression of IQSEC3 E749A (3.11 ± 0.17 for the first 60 min and 3.66 ± 0.27 for the next 60 min) (Figures 2B–2D). IQSEC3 KD decreased seizure latency, in association with an increase in the total time spent in seizures, both of which were normalized by expression of IQSEC3 WT, but not IQSEC3 E749A (Figures 2B, 2E, and 2F). Similar behavioral profiles of IQSEC3-KD mice were observed in the pilocarpine-induced epilepsy mouse model (Figure S3).

In line with these behavioral phenotypes, EEG and local field potential (LFP) recordings in IQSEC3-KD mice revealed higher amplitude and longer lasting KA-induced ictal activity compared with control mice (Figure 2G). Moreover, the number of seizure events per hour, determined from EEG activity, was significantly increased in IQSEC3-KD mice compared with control mice. The number of interictal spikes, quantified from 240 min of EEG recordings, was higher in IQSEC3-KD mice than in control mice (Figure 2H). This increased frequency of interictal spikes in IQSEC3-KD mice was rescued by coexpression of IQSEC3 WT but not IQSEC3 E749A (Figure 2H). Consistent with EEG recordings, the duration of interictal events was increased in LFP recordings in IQSEC3-KD mice compared with control mice, an effect that was completely normalized

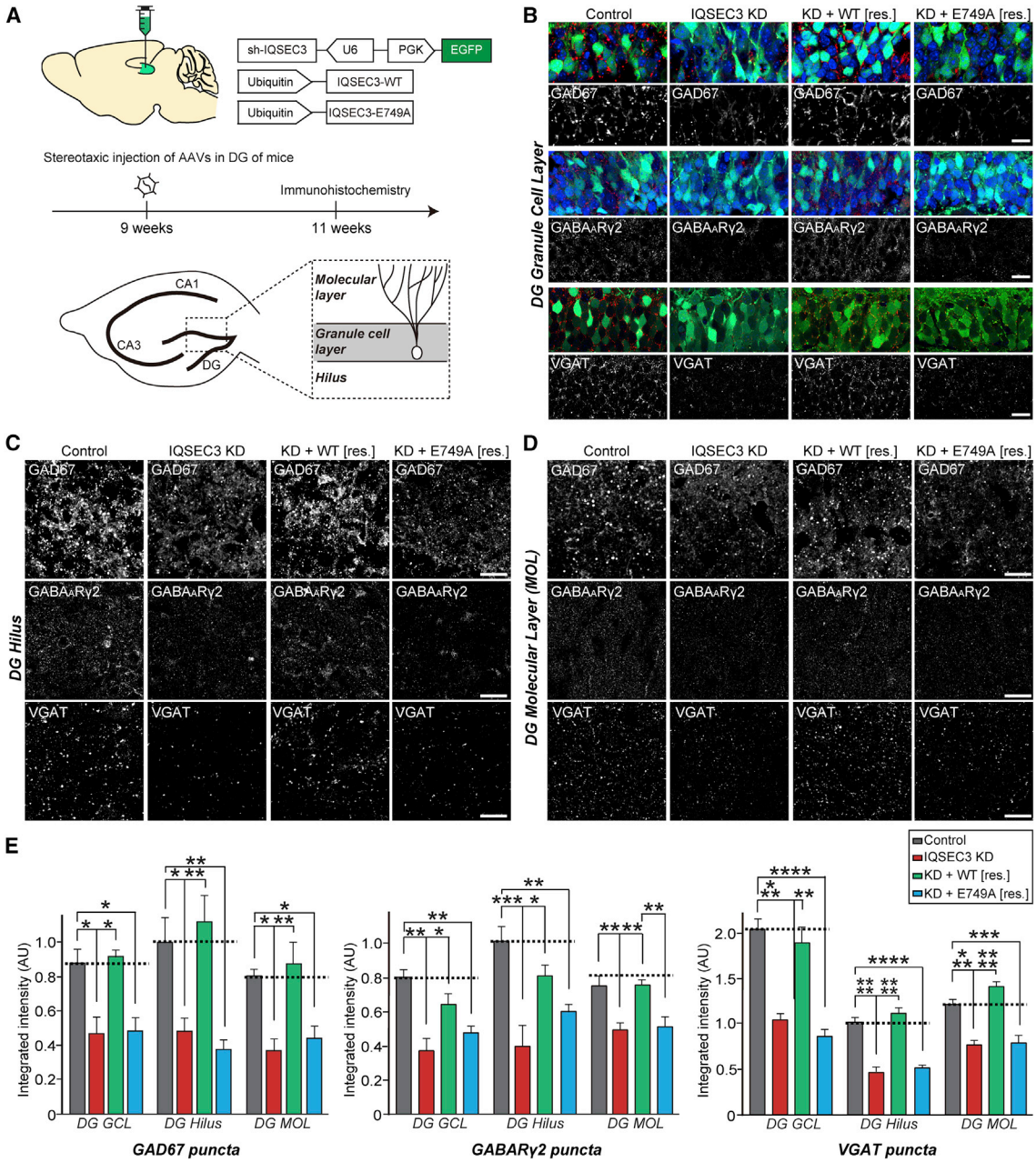

Figure 1. IQSEC3 KD in Mice Leads to Impaired GABAergic Synapse Maintenance in the DG

(A) Experimental protocols for quantitative immunohistochemistry experiments.

(B–D) Effects of IQSEC3 KD on synapse puncta in the DG granule cell layer (B), DG hilus (C), and DG molecular layer (MOL) (D). Representative images showing a reduction in GAD67, VGAT, or $GABA_AR\gamma2$ puncta intensity (red) in the DG in IQSEC3-KD neurons. Brain sections were immunostained for EGFP to show AAV-infected neurons (green) and counterstained with DAPI to show cell nuclei (blue). Scale bar, 10 μm.

(E) Quantification of GAD67, VGAT, and $GABA_AR\gamma2$ puncta intensity per tissue area (mean ± SEM; n = 8 mice each after averaging data from four sections/mouse; *p < 0.05, **p < 0.01, ***p < 0.001, and ****p < 0.0001 versus controls).

by coexpression of IQSEC3 WT but not IQSEC3 E749A (Figures 2I and 2J). Spectrograms for LFP signals after KA injection confirmed the enhanced power of high-frequency seizure activity in IQSEC3-KD mice, an effect that was again reversed by co-expression of IQSEC3 WT but not IQSEC3 E749A (Figure 2K). There are three well-characterized types of hippocampal oscillations representing seizure activity, theta (3–5 Hz), fast gamma (55–80 Hz), and slow gamma (30–45 Hz); disturbances in theta and gamma rhythm coherence, in particular, are observed in TLE and Alzheimer's disease (Buzsáki and Silva, 2012). Strikingly, normalized power spectral densities of theta (68.06 ± 7.39) and fast gamma (130.44 ± 19.50), but not slow gamma

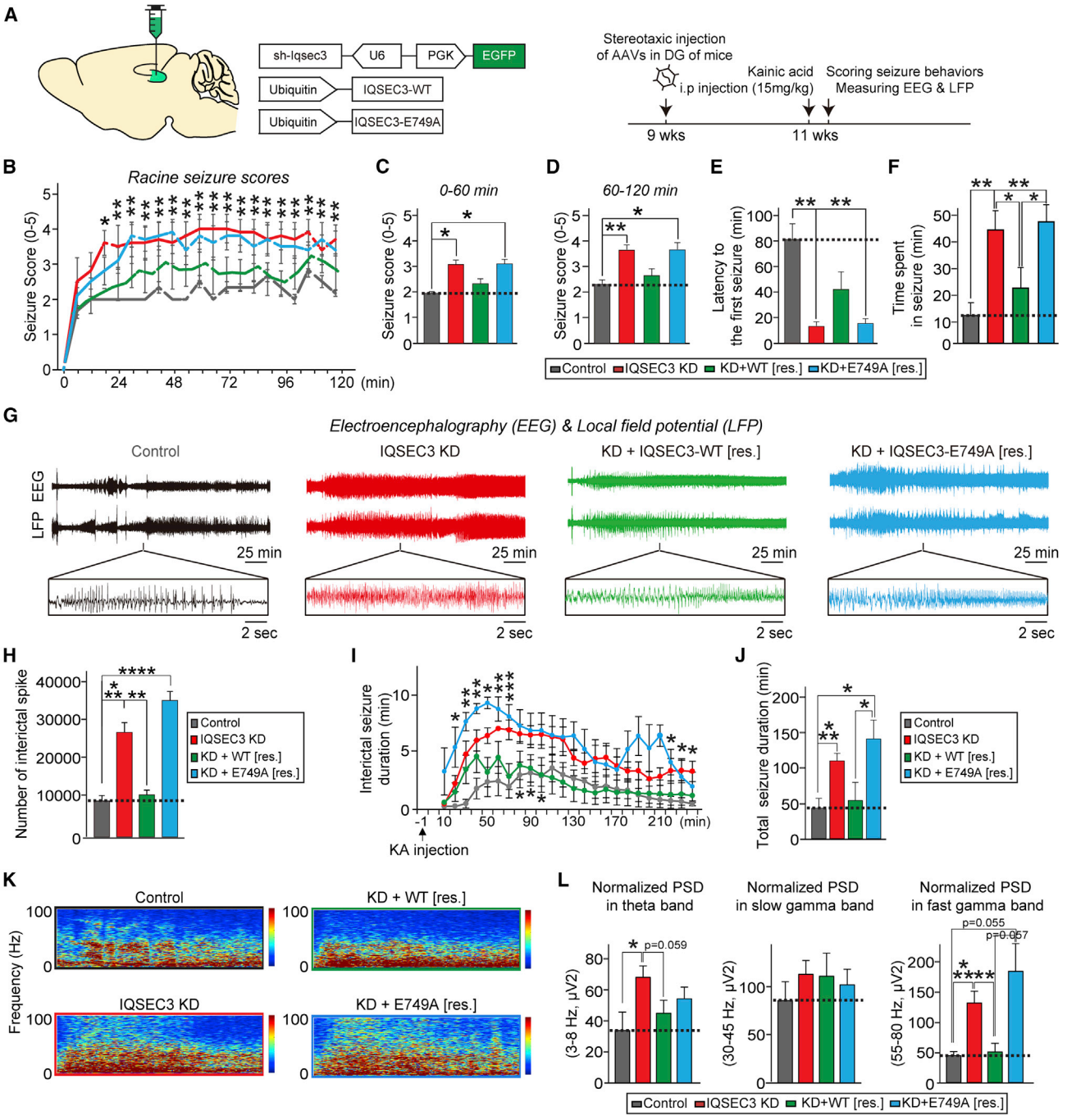

Figure 2. IQSEC3 KD Increases Induced Seizure Susceptibility in an ARF-GEF Activity-Dependent Manner

(A) Experimental scheme for seizure scoring and EEG recordings.

(B) KA-induced seizures in mice injected with the indicated AAVs were scored every 3 min for a total of 120 min, as described in Method Details in the STAR Methods (mean ± SEM; control, n = 11; IQSEC3 KD, n = 10; KD + WT [res.], n = 9; and KD + E749A [res.], n = 10 mice; *p < 0.05 and **p < 0.01 versus control).

(C and D) Quantification of mean score values for the first 60 min (C) and second 60 min (D) (n = 9–11 mice/condition; *p < 0.05 and **p < 0.01 versus controls).

(E) Quantification of latency to the first seizure after KA administration (n = 9–11 mice/condition; **p < 0.01).

(F) Quantification of time spent in seizure (n = 9–11 mice/condition; *p < 0.05 and **p < 0.01).

(G) Representative EEG and LFP traces. The expanded DG LFP traces in black boxes show typical epileptic seizure patterns after KA injection.

(H) The number of interictal events during 4 h, quantified from EEG signals (n = 8–11 mice/condition; **p < 0.01, ***p < 0.001, and ****p < 0.0001).

(I) Time course of seizure activity in the DG LFP after KA injection (mean ± SEM; control, n = 11; IQSEC3 KD, n = 10; KD + WT [res.], n = 9; and KD + E749A [res.], n = 10 mice; *p < 0.05, **p < 0.01, and ***p < 0.001 versus controls).

(legend continued on next page)

(30–45 Hz), bands were significantly increased in IQSEC3-KD mice compared with control mice (theta, 33.83 ± 11.89; fast gamma, 44.12 ± 6.36) (Figure 2L). The enhanced power in fast gamma bands observed in IQSEC3-KD mice was reversed to control level by coexpression of IQSEC3 WT (fast gamma, 50.10 ± 14.22), but not IQSEC3 E749A (fast gamma, 182.37 ± 45.88) (Figure 2L). The increased power in theta bands in IQSEC3-KD mice appeared to be rescued (i.e., not statistically different from controls) by coexpression of IQSEC3 WT or IQSEC3 E749A (Figure 2L). Collectively, our data suggest that the ARF-GEF activity of IQSEC3 is crucial for its anti-epileptic function.

IQSEC3 Deletion in the Hippocampal DG Induces Depletion of SST Peptides

There are scattered reports that SST^+-INs in the DG hilus are lost in patients with TLE and in animal models of this condition (de Lanerolle et al., 1989; Kumar and Buckmaster, 2006). Thus, we first quantified the number of neurons in the DG hilus of IQSEC3-deficient mice that show positive immunostaining for GAD67, SST, parvalbumin (PV), cholecystokinin (CCK), or calretinin (Figure 3A). We found that the number of DG hilar GABAergic interneurons ($GAD67^+$-INs) was profoundly decreased in IQSEC3-KD mice compared with control mice (Figures 3B and 3C). Specifically, the number of SST^+ immunoreactive neurons was specifically and profoundly decreased in the DG hilus of IQSEC3-KD mice (Figures 3D–3K). This selective reduction of the GABAergic cell type in the DG of IQSEC3-KD mice was completely rescued by coexpression of IQSEC3 WT but not IQSEC3 E749A (Figures 3B–3K), suggesting that it derives from a specific effect of IQSEC3 KD.

The reduced SST^+ immunoreactivity observed in the DG hilus of IQSEC3-KD mice might reflect selective death of SST^+-INs, loss of SST peptides in the SST^+-INs, or both. To assess these possibilities, we injected IQSEC3-KD AAVs into the DG of Sst-IRES-Cre mice (knockin mice expressing Cre recombinase in SST^+-INs) crossed with the $Rosa26^{LSL\text{-}tdTomato}$ (Ai9) reporter line, which selectively and robustly expresses tdTomato fluorescence in SST^+-INs (Figure 3L). We found that IQSEC3 KD did not alter the number of cells with tdTomato fluorescence (Figures 3M and 3N) but significantly decreased SST^+ immunoreactivity in tdTomato-positive SST^+-INs (Figures 3O and 3P), suggesting that IQSEC3 KD depletes SST peptides in the DG hilus of mice, rather than inducing a loss of SST^+-INs. However, IQSEC3 KD did not influence the expression levels of SST receptor 2 (SSTR2) and SST receptor 4 (SSTR4), which are abundantly expressed in hippocampal DG neurons (Moneta et al., 2002; Figure S4). Collectively, these data suggest that an IQSEC3 deficiency accelerates the onset of epileptic seizures, presumably through the concerted actions of a decreased number of functional GABAergic synapses and loss of SST peptides as a result of disrupted ARF signaling.

Expression of SST in DG-Specific IQSEC3-KD Mice Rescues Deficits in GABAergic Synapse Density and Enhanced Seizure Susceptibility

To directly assess whether the reduction in SST level observed in DG-specific IQSEC3-KD mice causes IQSEC3 KD-induced pathological phenotypes, we transduced Sst-*IRES*-Cre mice with empty AAVs (control) or IQSEC3 KD or cotransduced them with IQSEC3 KD and double-floxed, inverted open reading frame (DIO) Cre-dependent AAVs expressing full-length human SST14, the predominant form of SST in the central nervous system (Figure 4A). We confirmed that the AAV-DIO-hSST viral vector promoted selective expression of SST in neurons derived from Sst-IRES-Cre mice (Figure S5). Strikingly, restricted expression of SST in SST^+-INs remarkably ameliorated the impaired GABAergic synapse maintenance in granular cell and molecular layers of the DG in IQSEC3-KD mice (Figures 4B–4E). Moreover, restricted introduction of SST into SST^+-INs rescued the decreased amplitude of evoked inhibitory postsynaptic currents (eIPSCs) in granule neurons of DG-specific IQSEC3-KD mice (Figures 4F–4H). Surprisingly, there were marked increases in the frequency and amplitude of miniature inhibitory postsynaptic currents (mIPSCs), whereas there was no change in the frequency or amplitude of miniature excitatory postsynaptic currents (mEPSCs) in the DG-specific IQSEC3-KD mice (Figure S5). Consistent with this, the same molecular manipulations in IQSEC3-KD mice prevented the occurrence of KA-induced seizures, reducing them to a level similar to that observed in control mice (Figures 4I–4L). EEG recordings consistently showed that the increased number of ictal and interictal events per hour and longer seizure duration in IQSEC3-KD mice were rescued by restricted expression of SST in SST^+-INs (Figures 4M–4Q). Taken together, our results suggest that expression of SST peptides *per se* is sufficient to reverse the altered cellular pathophysiologies found in IQSEC3-KD mice and that SST peptides support the maintenance of IQSEC3-mediated GABAergic synapse and network activity.

SST Promotes Accumulation of Surface $GABA_A$ Receptors in Cultured Hippocampal Neurons

To further delineate how SST peptide is able to restore the impaired GABAergic synapse maintenance and enhanced seizures in the IQSEC3-KD mice, we probed the effect of SST action on surface $GABA_A$ receptor level in cultured hippocampal neurons. Incubation of the SST peptides for 2 h significantly increased the puncta density of surface $GABA_AR\gamma2$ (Figure S6). The increased surface $GABA_AR\gamma2^+$ puncta by SST treatment was completely abrogated by cotreatment of cyclosomatostatin (10 μM; a SST antagonist) or SecinH3 (30 μM; an inhibitor of the cytohesin ARF-GEF family), suggesting a molecular model whereby SST secretion from SST^+ INs might activate SSTRs, followed by positively facilitating the surface accumulation of $GABA_AR\gamma2$, possibly via mechanisms involving ARF signaling cascades (Figure S6).

(J) Total duration of seizures in the DG LFP over 240 min (mean ± SEMs; n = 8–11 mice/condition; *p < 0.05 and ***p < 0.001).

(K) Representative spectrograms in the DG LFP signal after KA injection.

(L) Normalized power spectral density for theta (3–5 Hz), slow gamma (30–45 Hz), and fast gamma (55–80 Hz) frequency bands (mean ± SEM; control, n = 8; IQSEC3 KD, n = 7; KD + WT [res.], n = 8; and KD + E749A [res.], n = 4 mice; *p < 0.05, **p < 0.01, and ***p < 0.005).

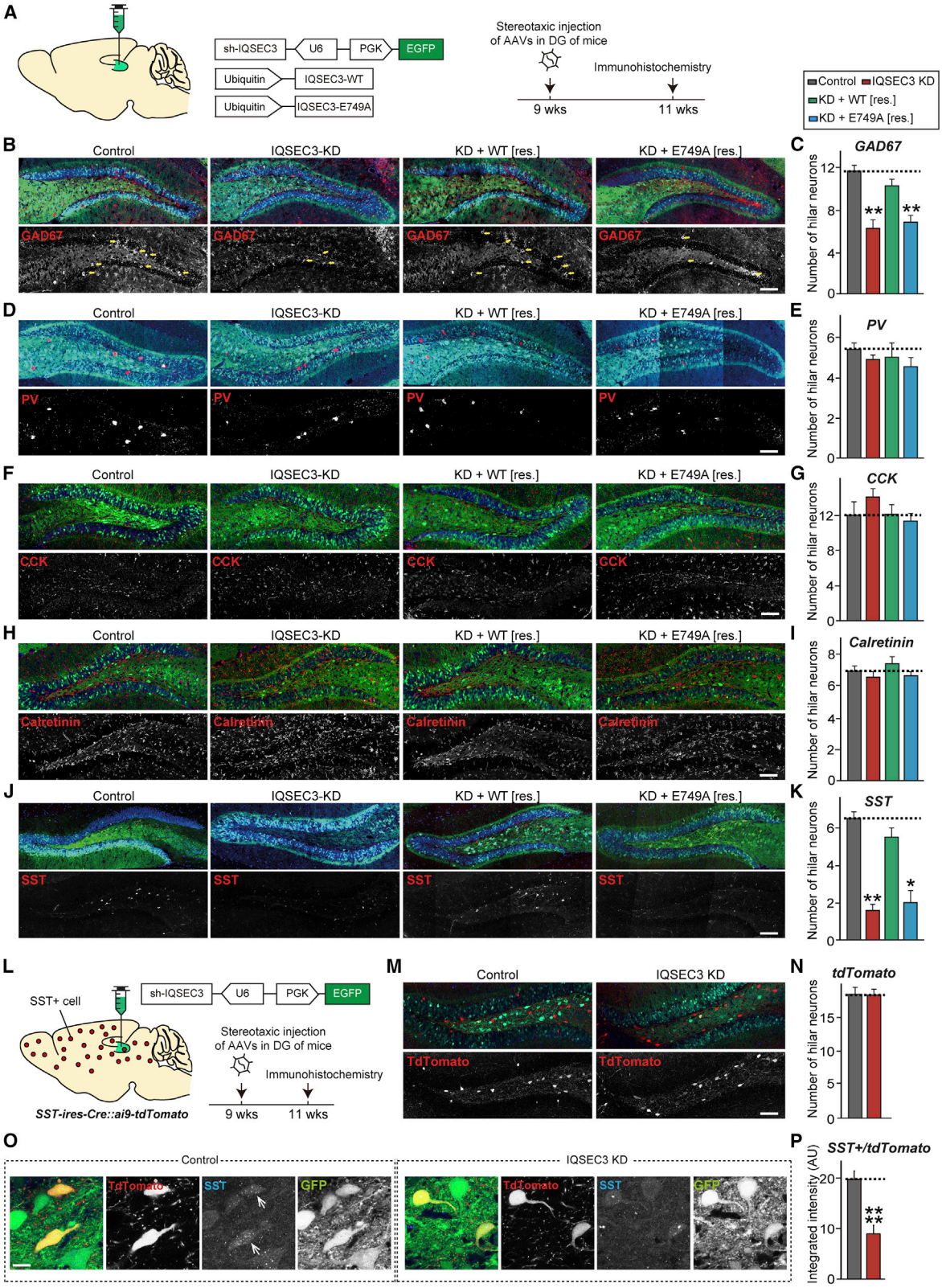

(legend on next page)

DISCUSSION

Here, we present a series of experiments that provide evidence that IQSEC3 is a key factor in controlling network activity in the hippocampus under both physiological and pathological conditions. Using molecular replacement experiments *in vivo*, we found that KD-based IQSEC3 loss of function triggered a variety of molecular and cellular alterations that frequently manifest in numerous animal models of TLE and in human epilepsy patients. We focused on the hippocampal DG in the present study because it has historically served as a model for use in extracting key hypothetical mechanisms underlying epileptogenesis (Dudek and Sutula, 2007). Because a subset of these key characteristics have been repeatedly reported in animal models deficient for the expression of GABAergic synaptic molecules (Ko et al., 2015), our results reinforce the concept that IQSEC3 is a central scaffold in GABAergic postsynaptic neurons and that its ARF-GEF activity is required for most, if not all, functional aspects examined.

We first demonstrated that IQSEC3 is required for GABAergic synapse maintenance *in vivo*. IQSEC3 KD produces a reduced number of GABAergic presynaptic terminals and postsynaptic $GABA_A$ receptors, at least in cultured hippocampal neurons (Um et al., 2016a) and hippocampal DG region, effects that are likely to elicit both spontaneous and KA-induced epileptic seizure development (Figure 2). In line with previous *in vitro* results (Um et al., 2016a), we found that IQSEC3 requires its ARF-GEF activity to orchestrate GABAergic synapse maintenance and network activity *in vivo* (Figures 1, 2, and 3). Consistent with this, recent studies showed that ARF6 activation by IQSEC3 is required for the correct alignment of pre- and postsynaptic specializations at GABAergic synapses (Früh et al., 2018) and that active ARF6 plays an important role in GABAergic synapse development (Kim et al., 2020).

Selective depletion of SST peptides was observed in DG-specific IQSEC3-KD mice (Figures 3 and 4). Induction of SST expression in SST^+-INs in the DG hilus completely reversed the enhanced seizure susceptibility, reduced GABAergic synapse puncta intensity, decreased GABAergic synaptic strength, and even increased the spontaneous GABAergic synaptic transmission characteristic of IQSEC3-KD mice (Figures 4 and S5). Although variability of mIPSC conductance in epileptic DG granule neurons has been reported, it is possible that augmented tonic inhibition keeps in check the enhanced excitatory drive or altered distribution of $GABA_A$Rs in IQSEC3-deficient DG granule neurons (Gibbs et al., 1997; Buhl et al., 1996; Cohen et al., 2003). Regardless of the precise mechanisms, introduction of SST into SST^+-INs completely compromised the IQSEC3-KD-induced phenotype. SST has long been implicated in epilepsy, on the basis of evidence for activity-dependent SST release during seizures, modulation of SST expression, and potent effects of SST on seizure control (Tallent and Qiu, 2008). Secreted SST peptides activate SSTRs, particularly those in mouse DG neurons (likely SSTR4; Moneta et al., 2002); these pervasive anti-convulsant effects reduce the number of excitatory synapses (Hou and Yu, 2013) and/or diminish presynaptic glutamate release within the hippocampus (Boehm and Betz, 1997). However, prior studies have not clearly defined the molecular mechanism(s) at GABAergic synapses that link the seizure rescuing effect of SSTR activation with other seizure-related pathologies. Because introduction of SST peptides is capable of functionally recovering the pathological phenotypes induced by IQSEC3 KD, it is tempting to speculate that SST expression induces hyperpolarization of target granule neurons by binding to SSTRs through a slow, but long-lasting, inhibitory mechanism (Liguz-Lecznar et al., 2016). It is obvious that activation of SSTRs are directly responsible for promoting surface accumulation of $GABA_A$ receptors, as treatment of the SSTR antagonist completely abrogated the effect of the SST peptides (Figure S6). SSTRs are members of the G protein-coupled receptor superfamily that couple to different G-protein subunits ($G_{i\alpha1}$, $G_{i\alpha3}$, and $G_{o\alpha}$) to mediate diverse signal transduction pathways (Lahlou et al., 2004). This intracellular signal transduction mechanism may be instrumental to the action of SSTRs in the current context, but how SSTRs and ARFs are molecularly linked remains to be determined. Alternatively, signaling crosstalk at glutamatergic and GABAergic synapses initiated by SST secretion and expression may contribute to this process, as supported by the previous observation that SSTRs directly interact with Shank family of excitatory scaffold proteins (Csaba and Dournaud, 2001; Sala et al., 2015). Because the ARF-GEF activity of IQSEC3 is essential for the integrity of SST^+-INs (Figure 3), restoration of impaired GABAergic synapse maintenance may be the pivotal step in the chain of events that rescues the regulation of SST^+-INs survival and seizure susceptibility. Another area of future investigation should be to understand how loss of SST peptides is triggered by IQSEC3 deficiency. Addressing this important question

Figure 3. IQSEC3 Deficiency Reduces SST Expression in an ARF-GEF Activity-Dependent Manner

(A) Experimental scheme for immunohistochemical analyses.

(B–K) Representative images showing the numbers of $GAD67^+$ (B), PV^+ (D), CCK^+ (F), $calretinin^+$ (H), and SST^+ (J) neurons in DG hilus of mice injected with the indicated AAVs. Brain sections were immunostained for EGFP (green) to identify neurons infected with the indicated AAVs or with antibodies against the indicated cell type-specific markers (red) and counterstained with DAPI (blue). Scale bar, 100 μm. The numbers of $GAD67^+$ (C), PV^+ (E), CCK^+ (G), $calretinin^+$ (I), and SST^+ (K) neurons in DG hilus was quantitated (mean ± SEM; n = 5 mice for all conditions; $^*p < 0.05$ and $^{**}p < 0.01$ versus controls).

(L) Experimental scheme for immunohistochemical analyses presented in (M)–(P).

(M) Representative images showing the number of cells with tdTomato fluorescence in DG hilus. Brain sections were immunostained for EGFP (green) to identify neurons infected with AAVs and counterstained with DAPI (blue). Scale bar, 100 μm.

(N) Number of cells with tdTomato fluorescence in DG hilus was quantitated (mean ± SEM; n = 3 mice each after averaging data from six sections/mouse).

(O) Representative images showing SST expression in $tdTomato^+$ cells in DG hilus. Brain sections were immunostained for EGFP (green) to identify neurons infected with AAVs and SST (blue) to label SST peptides. Scale bar, 20 μm.

(P) Integrated intensity of SST fluorescence in $tdTomato^+$ cells in DG hilus was quantitated (mean ± SEM; n = 3 mice each after averaging data from six sections/mouse; $^{****}p < 0.0001$ versus control).

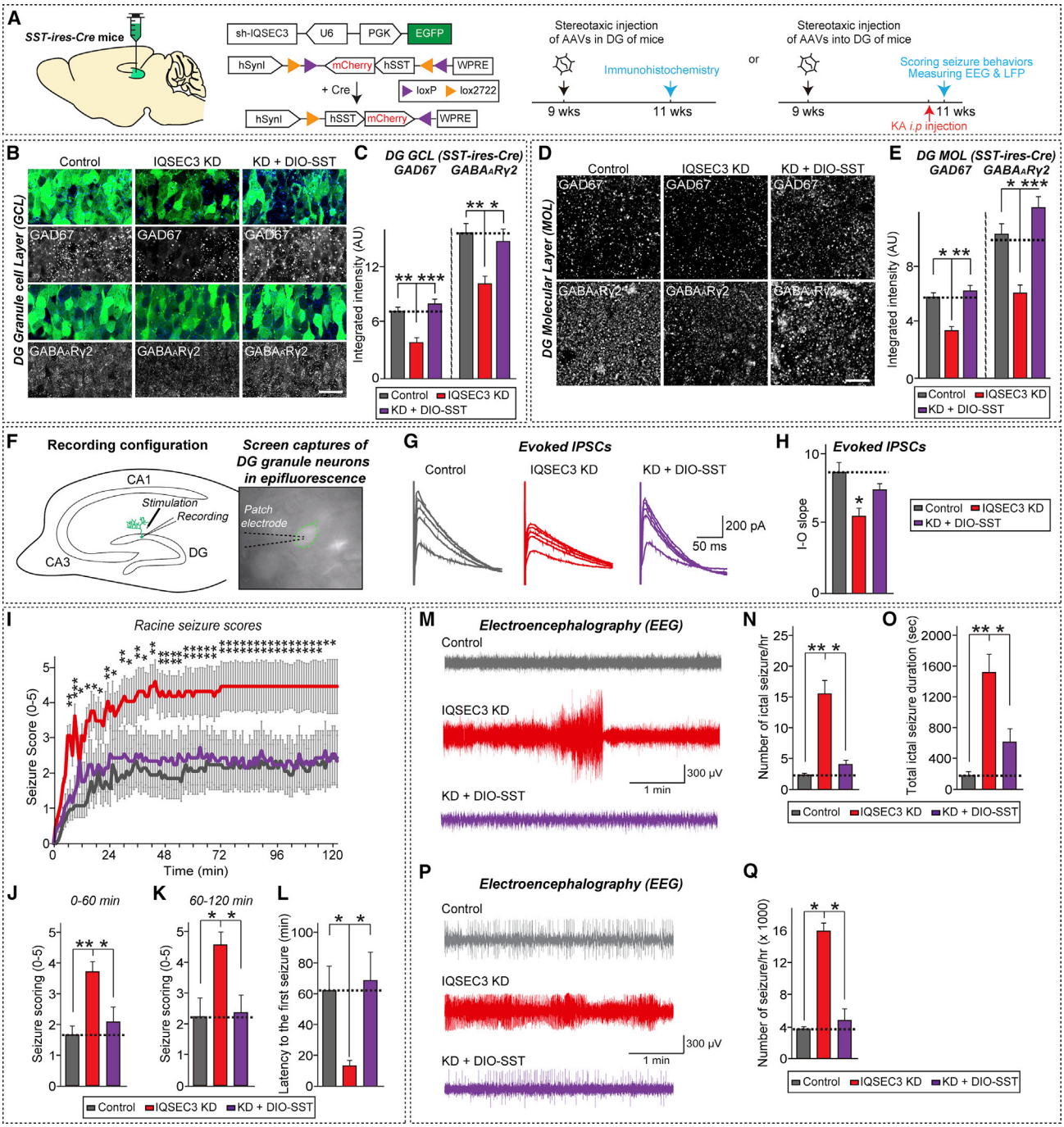

Figure 4. Expression of SST Peptides Normalizes GABAergic Synaptic Deficits and Increased Seizure Susceptibility Triggered by IQSEC3 KD

(A) Experimental scheme for immunohistochemistry, electrophysiology, seizure-scoring analyses, and EEG recordings presented in (B)–(Q).

(B and D) Representative images of the hippocampal DG granular cell layer (GCL) (B) or DG molecular layer (MOL) (D) of *Sst*-IRES-Cre mice 2 weeks after injection of the indicated AAVs. Brain sections were immunostained for EGFP (green) to show neurons infected with indicated AAVs and with antibodies to anti-GAD67 or anti-$GABA_AR\gamma2$ (red). Scale bar: 20 μm.

(C and E) Quantification of the integrated intensity of GAD67 and GABARγ2 immunoreactivities in the DG GCL (C) and MOL (E) (mean ± SEM; n = 6 mice each after averaging data from four sections/mouse; *p < 0.05, **p < 0.01, and ***p < 0.001).

(F) Schematic configuration of electrophysiological recordings presented in (G) and (H).

(G and H) Representative eIPSC traces (G) recorded from DG granule neurons in acute DG slices from *Sst*-IRES-Cre mice injected with the indicated AAVs. Bar graphs (H) show summary of fitted linear input/output slopes (mean ± SEM; control, n = 13 cells/4 mice; IQSEC3 KD, n = 17 cells/5 mice; and + DIO-SST, n = 18 cells/5 mice; *p < 0.05 versus control).

(legend continued on next page)

using conditional knockout mice deficient for IQSEC3 expression, selectively in SST^+-INs, is warranted.

Because increased intracellular Ca^{2+} concentration and activation of CREB (cyclic AMP-responsive element binding protein) and BDNF (brain-derived neurotrophic factor) were previously reported to regulate SST gene transcription (Sánchez-Muñoz et al., 2010, 2011), it is plausible that network hyperactivity triggered by IQSEC3 loss abnormally orchestrates the machinery involved in the transcription of SST genes, leading to depletion of SST peptides. Importantly, dysregulation of ARF signaling cascades upon IQSEC3 deletion could negatively affect SST secretion or accelerate the degradation of SST peptides. Together with other interneuron types, SST^+-INs have been strongly implicated in seizure disorders that feature recurrent elevated activity in neuronal networks (Urban-Ciecko and Barth, 2016). Moreover, using various models of epilepsy, previous reports have shown that SST^+-INs in the DG hilus receive stronger excitatory input compared with healthy animals, a difference that may alter the ability to synchronize network inhibition (Grosser et al., 2014; Halabisky et al., 2010; Zhang et al., 2009). Thus, the increased seizure susceptibility of IQSEC3-KD mice observed in the KA-induced epilepsy model could reflect the loss of GABAergic synaptic inhibition and network hyperexcitability prior to seizure onset, similar to that shown in a genetic model of cortical malformation (Trotter et al., 2006). Surprisingly, the relationship between SST peptides and GABAergic synapse maintenance and/or epileptogenesis has been largely elusive. On the basis of previous studies (Früh et al., 2018; Um et al., 2016a), it is likely that although IQSEC3 KD-induced seizures ultimately derive from an imbalanced E/I ratio initially triggered by the loss of GABAergic postsynaptic organizer IQSEC3, depletion of SST peptides may further aggravate the severity of various pathophysiological phenotypes, underscoring the crucial role of SST in regulating GABAergic synapse maintenance. The N-terminal G-domain of gephyrin is required not only for gephyrin trimerization but also for binding to IQSEC3 to promote GABAergic synapse development. Because IQSEC3 is required for gephyrin clustering in cultured hippocampal neurons (Um et al., 2016a), it is tempting to suggest that the interaction of gephyrin with IQSEC3 is critical for formation of gephyrin trimers, which provide protection against degradation resulting from seizure-related network hyperactivity and excitotoxicity (Agarwal et al., 2008; Costa et al., 2016). On the basis of the present findings, it is plausible that impairment of IQSEC3 binding to gephyrin G-domain mutants associated with epilepsy could lead to defective ARF signaling, deficits in GABAergic synapse maintenance, decreased SST expression, and network dysfunction in a sequential manner, which collectively may explain how gephyrin mutants with irregular exon skipping in the G-domain observed in TLE patients are linked to the etiology of the disease. Thus, our data suggest the potential of SST peptides, through their ability to regulate GABAergic synapse maintenance through enhanced surface trafficking of $GABA_A$ receptors to form the basis for a novel therapeutic strategy for effective epilepsy treatment.

In sum, our study provides framework for monitoring early, specific molecular epileptogenic events on the basis of novel mechanisms involving IQSEC3-mediated molecular components (Dobolyi et al., 2014). Future efforts using IQSEC3-conditional knockout mice are warranted to validate findings on the basis of IQSEC3 KD and identify key neural circuits in the DG and other brain regions that underlie IQSEC3-KD-relevant epileptogenesis mechanisms.

STAR★METHODS

Detailed methods are provided in the online version of this paper and include the following:

- KEY RESOURCES TABLE
- LEAD CONTACT AND MATERIALS AVAILABILITY
- EXPERIMENTAL MODEL AND SUBJECT DETAILS
  - Cell Culture
  - Animals
- METHOD DETAILS
  - Construction of Expression Vectors
  - Antibodies
  - ARF6 Activation Assay
  - Production of Recombinant Adeno-associated Viruses (AAVs)
  - Stereotaxic Surgery and Virus Injections
  - Seizure Behavior Scoring
  - EEG Recordings and Analyses
  - Local Field Potential (LFP) Recordings and Analyses
  - Immunohistochemistry and Imaging
  - Electrophysiology
  - Neuron Culture, Imaging, and Quantification
- QUANTIFICATION AND STATISTICAL ANALYSIS
- DATA AND CODE AVAILABILITY

SUPPLEMENTAL INFORMATION

Supplemental Information can be found online at https://doi.org/10.1016/j.celrep.2020.01.053.

(I) KA-induced seizures were scored every 3 min for a total of 120 min (mean ± SEM; control, n = 10; IQSEC3-KD, n = 7; IQSEC3-KD + DIO-SST, n = 9 mice; *p < 0.05 and **p < 0.01 versus control)
(J and K) Quantification of mean score values for the first 60 min (J)and second 60 min (K) (n = 7–10 mice/condition; *p < 0.05 and **p < 0.01 versus control).
(L) Quantification of latency to the first seizure after KA administration (n = 7–10 mice/condition; *p < 0.05 versus control).
(M) Representative EEG traces of ictal-like seizures recorded from the cortex.
(N) and (O) Quantification of the number of ictal-like seizures (N) and total duration of ictal-like seizures (O) per hour (n = 8–11 mice/condition; *p < 0.05 and **p < 0.01 versus control).
(P) Representative EEG traces of interictal events recorded from the cortex.
(Q) Quantification of the number of interictal events (n = 5 or 6 mice/condition; *p < 0.05 versus control).

ACKNOWLEDGMENTS

We are grateful to Dr. Hiroyuki Sakagami (Kitasato University, Japan) for kind gifts of IQSEC3 antibody and Jinha Kim for technical assistance. This study was supported by grants from the National Research Foundation of Korea (NRF) funded by the Ministry of Science and ICT (2019R1H1A2079884 to J.W.U.) and the Brain Research Program through the NRF funded by the Ministry of Science, ICT & Future Planning (2017M3C7A1023470 to J. Ko and 2017M3C7A1023471 to E.C.).

AUTHOR CONTRIBUTIONS

J. Ko and J.W.U. conceived the project. S.K., H.K., D.P., J. Kim, J.H., J.S.K., H.J., and D.K. performed the experiments. S.K., H.K., D.P., J. Kim, J.H., E.C., J. Ko, and J.W.U. analyzed the data. E.C., J. Ko, and J.W.U. wrote the manuscript with input from the other authors.

DECLARATION OF INTERESTS

The authors declare no competing interests.

Received: September 13, 2019
Revised: December 28, 2019
Accepted: January 16, 2020
Published: February 11, 2020

REFERENCES

Agarwal, S., Tannenberg, R.K., and Dodd, P.R. (2008). Reduced expression of the inhibitory synapse scaffolding protein gephyrin in Alzheimer's disease. J. Alzheimers Dis. *14*, 313–321.

Alvarez, F.J. (2017). Gephyrin and the regulation of synaptic strength and dynamics at glycinergic inhibitory synapses. Brain Res. Bull. *129*, 50–65.

Baraban, S.C., Southwell, D.G., Estrada, R.C., Jones, D.L., Sebe, J.Y., Alfaro-Cervello, C., García-Verdugo, J.M., Rubenstein, J.L., and Alvarez-Buylla, A. (2009). Reduction of seizures by transplantation of cortical GABAergic interneuron precursors into Kv1.1 mutant mice. Proc. Natl. Acad. Sci. U S A *106*, 15472–15477.

Boehm, S., and Betz, H. (1997). Somatostatin inhibits excitatory transmission at rat hippocampal synapses via presynaptic receptors. J. Neurosci. *17*, 4066–4075.

Buhl, E.H., Otis, T.S., and Mody, I. (1996). Zinc-induced collapse of augmented inhibition by GABA in a temporal lobe epilepsy model. Science *271*, 369–373.

Buzsáki, G., and Silva, F.L. (2012). High frequency oscillations in the intact brain. Prog. Neurobiol. *98*, 241–249.

Choi, S., Ko, J., Lee, J.R., Lee, H.W., Kim, K., Chung, H.S., Kim, H., and Kim, E. (2006). ARF6 and EFA6A regulate the development and maintenance of dendritic spines. J. Neurosci. *26*, 4811–4819.

Choii, G., and Ko, J. (2015). Gephyrin: a central GABAergic synapse organizer. Exp. Mol. Med. *47*, e158.

Cohen, A.S., Lin, D.D., Quirk, G.L., and Coulter, D.A. (2003). Dentate granule cell GABA(A) receptors in epileptic hippocampus: enhanced synaptic efficacy and altered pharmacology. Eur. J. Neurosci. *17*, 1607–1616.

Costa, J.T., Mele, M., Baptista, M.S., Gomes, J.R., Ruscher, K., Nobre, R.J., de Almeida, L.P., Wieloch, T., and Duarte, C.B. (2016). Gephyrin cleavage in in vitro brain ischemia decreases GABAA receptor clustering and contributes to neuronal death. Mol. Neurobiol. *53*, 3513–3527.

Csaba, Z., and Dournaud, P. (2001). Cellular biology of somatostatin receptors. Neuropeptides *35*, 1–23.

de Lanerolle, N.C., Kim, J.H., Robbins, R.J., and Spencer, D.D. (1989). Hippocampal interneuron loss and plasticity in human temporal lobe epilepsy. Brain Res. *495*, 387–395.

Dobolyi, A., Kékesi, K.A., Juhász, G., Székely, A.D., Lovas, G., and Kovács, Z. (2014). Receptors of peptides as therapeutic targets in epilepsy research. Curr. Med. Chem. *21*, 764–787.

Dudek, F.E., and Sutula, T.P. (2007). Epileptogenesis in the dentate gyrus: a critical perspective. Prog. Brain Res. *163*, 755–773.

Dudek, F.E., Yasumura, T., and Rash, J.E. (1998). 'Non-synaptic' mechanisms in seizures and epileptogenesis. Cell Biol. Int. *22*, 793–805.

Ellis, S.E., Panitch, R., West, A.B., and Arking, D.E. (2016). Transcriptome analysis of cortical tissue reveals shared sets of downregulated genes in autism and schizophrenia. Transl. Psychiatry *6*, e817.

Förstera, B., Belaidi, A.A., Jüttner, R., Bernert, C., Tsokos, M., Lehmann, T.N., Horn, P., Dehnicke, C., Schwarz, G., and Meier, J.C. (2010). Irregular RNA splicing curtails postsynaptic gephyrin in the cornu ammonis of patients with epilepsy. Brain *133*, 3778–3794.

Früh, S., Tyagarajan, S.K., Campbell, B., Bosshard, G., and Fritschy, J.M. (2018). The catalytic function of the gephyrin-binding protein IQSEC3 regulates neurotransmitter-specific matching of pre- and post-synaptic structures in primary hippocampal cultures. J. Neurochem. *147*, 477–494.

Gibbs, J.W., 3rd, Shumate, M.D., and Coulter, D.A. (1997). Differential epilepsy-associated alterations in postsynaptic GABA(A) receptor function in dentate granule and CA1 neurons. J. Neurophysiol. *77*, 1924–1938.

Groeneweg, F.L., Trattnig, C., Kuhse, J., Nawrotzki, R.A., and Kirsch, J. (2018). Gephyrin: a key regulatory protein of inhibitory synapses and beyond. Histochem. Cell Biol. *150*, 489–508.

Grosser, S., Queenan, B.N., Lalchandani, R.R., and Vicini, S. (2014). Hilar somatostatin interneurons contribute to synchronized GABA activity in an in vitro epilepsy model. PLoS ONE *9*, e86250.

Halabisky, B., Parada, I., Buckmaster, P.S., and Prince, D.A. (2010). Excitatory input onto hilar somatostatin interneurons is increased in a chronic model of epilepsy. J. Neurophysiol. *104*, 2214–2223.

Hiester, K.G., and Santy, L.C. (2013). The cytohesin coiled-coil domain interacts with threonine 276 to control membrane association. PLoS ONE *8*, e82084.

Hou, Z.H., and Yu, X. (2013). Activity-regulated somatostatin expression reduces dendritic spine density and lowers excitatory synaptic transmission via postsynaptic somatostatin receptor 4. J. Biol. Chem. *288*, 2501–2509.

Jefferys, J.G. (2010). Advances in understanding basic mechanisms of epilepsy and seizures. Seizure *19*, 638–646.

Kim, H., Jung, H., Jung, H., Kwon, S.K., Ko, J., and Um, J.W. (2020). The small GTPase ARF6 regulates GABAergic synapse development. Mol. Brain *13*, 2.

Ko, J., Choii, G., and Um, J.W. (2015). The balancing act of GABAergic synapse organizers. Trends Mol. Med. *21*, 256–268.

Ko, J., Kim, S., Valtschanoff, J.G., Shin, H., Lee, J.R., Sheng, M., Premont, R.T., Weinberg, R.J., and Kim, E. (2003). Interaction between liprin-alpha and GIT1 is required for AMPA receptor targeting. J. Neurosci. *23*, 1667–1677.

Ko, J., Soler-Llavina, G.J., Fuccillo, M.V., Malenka, R.C., and Südhof, T.C. (2011). Neuroligins/LRRTMs prevent activity- and Ca2+/calmodulin-dependent synapse elimination in cultured neurons. J. Cell Biol. *194*, 323–334.

Kumar, S.S., and Buckmaster, P.S. (2006). Hyperexcitability, interneurons, and loss of GABAergic synapses in entorhinal cortex in a model of temporal lobe epilepsy. J. Neurosci. *26*, 4613–4623.

Lahlou, H., Guillermet, J., Hortala, M., Vernejoul, F., Pyronnet, S., Bousquet, C., and Susini, C. (2004). Molecular signaling of somatostatin receptors. Ann. N Y Acad. Sci. *1014*, 121–131.

Leite, J.P., Neder, L., Arisi, G.M., Carlotti, C.G., Jr., Assirati, J.A., and Moreira, J.E. (2005). Plasticity, synaptic strength, and epilepsy: what can we learn from ultrastructural data? Epilepsia *46* (*Suppl 5*), 134–141.

Li, K., Zhou, T., Liao, L., Yang, Z., Wong, C., Henn, F., Malinow, R., Yates, J.R., 3rd, and Hu, H. (2013). βCaMKII in lateral habenula mediates core symptoms of depression. Science *341*, 1016–1020.

Liguz-Lecznar, M., Urban-Ciecko, J., and Kossut, M. (2016). Somatostatin and somatostatin-containing neurons in shaping neuronal activity and plasticity. Front. Neural Circuits *10*, 48.

Marriott, A.L., Rojas-Mancilla, E., Morales, P., Herrera-Marschitz, M., and Tasker, R.A. (2017). Models of progressive neurological dysfunction originating early in life. Prog. Neurobiol. *155*, 2–20.

Moneta, D., Richichi, C., Aliprandi, M., Dournaud, P., Dutar, P., Billard, J.M., Carlo, A.S., Viollet, C., Hannon, J.P., Fehlmann, D., et al. (2002). Somatostatin receptor subtypes 2 and 4 affect seizure susceptibility and hippocampal excitatory neurotransmission in mice. Eur. J. Neurosci. *16*, 843–849.

Racine, R.J. (1972). Modification of seizure activity by electrical stimulation. II. Motor seizure. Electroencephalogr. Clin. Neurophysiol. *32*, 281–294.

Sala, C., Vicidomini, C., Bigi, I., Mossa, A., and Verpelli, C. (2015). Shank synaptic scaffold proteins: keys to understanding the pathogenesis of autism and other synaptic disorders. J. Neurochem. *135*, 849–858.

Sánchez-Muñoz, I., Sánchez-Franco, F., Vallejo, M., Fernández, A., Palacios, N., Fernández, M., and Cacicedo, L. (2010). Activity-dependent somatostatin gene expression is regulated by cAMP-dependent protein kinase and Ca2+-calmodulin kinase pathways. J. Neurosci. Res. *88*, 825–836.

Sánchez-Muñoz, I., Sánchez-Franco, F., Vallejo, M., Fernández, A., Palacios, N., Fernández, M., Sánchez-Grande, M., and Cacicedo, L. (2011). Regulation of somatostatin gene expression by brain derived neurotrophic factor in fetal rat cerebrocortical cells. Brain Res. *1375*, 28–40.

Steinberg, E.E., Christoffel, D.J., Deisseroth, K., and Malenka, R.C. (2015). Illuminating circuitry relevant to psychiatric disorders with optogenetics. Curr. Opin. Neurobiol. *30*, 9–16.

Südhof, T.C. (2017). Molecular neuroscience in the 21st century: a personal perspective. Neuron *96*, 536–541.

Tallent, M.K., and Qiu, C. (2008). Somatostatin: an endogenous antiepileptic. Mol. Cell. Endocrinol. *286*, 96–103.

Trotter, S.A., Kapur, J., Anzivino, M.J., and Lee, K.S. (2006). GABAergic synaptic inhibition is reduced before seizure onset in a genetic model of cortical malformation. J. Neurosci. *26*, 10756–10767.

Um, J.W. (2017). Synaptic functions of the IQSEC family of ADP-ribosylation factor guanine nucleotide exchange factors. Neurosci. Res. *116*, 54–59.

Um, J.W., Choii, G., Park, D., Kim, D., Jeon, S., Kang, H., Mori, T., Papadopoulos, T., Yoo, T., Lee, Y., et al. (2016a). IQ motif and SEC7 domain-containing protein 3 (IQSEC3) interacts with gephyrin to promote inhibitory synapse formation. J. Biol. Chem. *291*, 10119–10130.

Um, J.W., Choi, T.Y., Kang, H., Cho, Y.S., Choii, G., Uvarov, P., Park, D., Jeong, D., Jeon, S., Lee, D., et al. (2016b). LRRTM3 regulates excitatory synapse development through alternative splicing and neurexin binding. Cell Rep. *14*, 808–822.

Urban-Ciecko, J., and Barth, A.L. (2016). Somatostatin-expressing neurons in cortical networks. Nat. Rev. Neurosci. *17*, 401–409.

Zhang, W., Yamawaki, R., Wen, X., Uhl, J., Diaz, J., Prince, D.A., and Buckmaster, P.S. (2009). Surviving hilar somatostatin interneurons enlarge, sprout axons, and form new synapses with granule cells in a mouse model of temporal lobe epilepsy. J. Neurosci. *29*, 14247–14256.

STAR★METHODS

KEY RESOURCES TABLE

REAGENT or RESOURCE	SOURCE	IDENTIFIER
Antibodies		
Rabbit polyclonal Anti-IQSEC3	Jaewon Ko's lab	JK079; RRID: AB_2687864
Mouse monoclonal Anti-GAD67	Millipore	Cat #MAB5406; RRID: AB_2278725
Rabbit monoclonal Anti-$GABA_AR\gamma2$	Synaptic Systems	Cat #224 003; RRID AB_2263066
Rabbit polyclonal Anti-VGAT	Synaptic Systems	Cat #131 003; RRID: AB_887869
Guinea pig polyclonal Anti-VGLUT1	Millipore	Cat #AB5905; RRID: AB_2301751
Mouse monoclonal Anti-PV	Swant	Cat #PV235; RRID: AB_10000343
Rat monoclonal Anti-SST	Millipore	Cat #MAB354; RRID: AB_2255365
Rabbit polyclonal Anti-CCK-8	Immunostar	Cat #20078; RRID: AB_572224
Mouse monoclonal Anti-Calretinin	Millipore	Cat #MAB1568; RRID: AB_94259
Rabbit polyclonal Anti-SSTR2	ThermoFisher	Cat #PA3-109; RRID: AB_2196063
Rabbit polyclonal Anti-SSTR4	ThermoFisher	Cat #PA3-111; RRID: AB_2196370
Goat polyclonal -Anti-EGFP	Abcam	Cat #ab5450; RRID: AB_304897
Rabbit polyclonal Anti-MAP2	Millipore	Cat #AB5622; RRID: AB_91939
Mouse monoclonal Anti-HA	Biolegend	Cat #MMS-101R-1000; RRID: AB_291262
Cy3-conjugated Donkey Anti-Rabbit IgG antibody	Jackson ImmunoResearch Laboratories	Cat #711-165-152; RRID: AB_2307443
Cy3-conjugated Donkey Anti-Mouse IgG antibody	Jackson ImmunoResearch Laboratories	Cat #715-165-150; RRID: AB_2340813
Cy3-conjugated Donkey Anti-guinea pig IgG antibody	Jackson ImmunoResearch Laboratories	Cat #706-165-148; RRID: AB_2340460
Cy3-conjugated Donkey Anti-Rat IgG antibody	Jackson ImmunoResearch Laboratories	Cat #712-165-150; RRID: AB_2340666
Cy5-conjugated Donkey Anti-Rat IgG antibody	Jackson ImmunoResearch Laboratories	Cat #711-175-152; RRID: AB_2340607
Chemicals, Peptides, and Recombinant Proteins		
SecinH3	Tocris	Cat #2849
Kainic acid	Sigma	Cat #K0250
Pilocarpine	Sigma	Cat #P6503
Neurobasal medium	ThermoFisher Scientific	Cat #21103049
B-27 supplement (50X)	ThermoFisher Scientific	Cat #17504-044
Pennicillin/Streptomycin	ThermoFisher Scientific	Cat #15140122
HBSS (Hanks' Balanced Salt Solution)	ThermoFisher	Cat #14065056
GlutaMax Supplement	ThermoFisher Scientific	Cat #35050061
FBS (Fetal Bovine Serum)	WELGENE	Cat #PK004-01
Sodium pyruvate	ThermoFisher Scientific	Cat #11360070
Poly-D-lysine hydrobromide	Sigma	Cat #P0899
Vectashield mounting medium	Vector Laboratories	Cat #H-1200
Somatostatin	Tocris	Cat #1157
Cyclosomatostatin	Tocris	Cat #3493
Experimental Models: Cell Lines		
Cultured neuronal cells (from rat embryos)	N/A	N/A
HEK293T cells	ATCC	Cat # CRL-3216
Experimental Models: Organisms/Strains		
Mouse: C57BL/6N mice	The Jackson Laboratory	Cat #005304
Mouse: *Sst*-IRES-Cre mice	The Jackson Laboratory	Cat #013044
Mouse: $Rosa26^{LSL\text{-}tdTomato}$ (Ai9) reporter line	The Jackson Laboratory	Cat #007905
Recombinant DNA		
pAAV-U6-EGFP	Cell Biolabs	Cat #VPK-413
pAAV-U6-sh-IQSEC3-EGFP	This study	N/A

(*Continued on next page*)

Continued

REAGENT or RESOURCE	SOURCE	IDENTIFIER
pAAV2/9-IQSEC3 WT	This study	N/A
pAAV2/9-IQSEC3 E749A	This study	N/A
pAAV2/9-hSyn-DIO-hSST-mCherry	This study	N/A
Software and Algorithms		
MetaMorph	Molecular Devices	https://www.moleculardevices.com
GraphPad Prism 7.0	GraphPad	https://www.graphpad.com

LEAD CONTACT AND MATERIALS AVAILABILITY

Further information and requests for resources and reagents should be directed to and will be fulfilled by the Lead Contact. Plasmids generated in this study are available from the Lead Contact, Ji Won Um (jiwonum@dgist.ac.kr), upon request. All unique/stable reagents generated in this study are available from the Lead Contact with a completed Materials Transfer Agreement.

EXPERIMENTAL MODEL AND SUBJECT DETAILS

Cell Culture

HEK293T cells were cultured in Dulbecco's Modified Eagle's Medium (DMEM; WELGENE) supplemented with 10% fetal bovine serum (FBS; Tissue Culture Biologicals) and 1% penicillin-streptomycin (Thermo Fisher) at 37°C in a humidified 5% CO_2 atmosphere. All procedures were performed according to the guidelines and protocols for rodent experimentation approved by the Institutional Animal Care and Use Committee of DGIST.

Animals

All C57BL/6N and *Sst*-IRES-Cre mice (purchased from Jackson Laboratory, ME, USA; stock number: 013044) were maintained and handled in accordance with protocols (DGIST-IACUC-19052109-00) approved by the Institutional Animal Care and Use Committee of DGIST under standard, temperature-controlled laboratory conditions. Mice were maintained on a 12:12 light/dark cycle (lights on at 6:00 am and off at 6:00 pm), and received water and food *ad libitum.* All experimental procedures were performed on male mice. Pregnant rats purchased from Daehan Biolink were used for *in vitro* culture of dissociated cortical or hippocampal neurons. All procedures were conducted according to the guidelines and protocols for rodent experimentation approved by the Institutional Animal Care and Use Committee of DGIST. All procedures were conducted according to the guidelines and protocols for rodent experimentation approved by the Institutional Animal Care and Use Committee of DGIST. All experimental procedures were performed on male mice. There was no specific reason for rejecting female mice in the current study apart from a general desire to minimize experimental variability.

METHOD DETAILS

Construction of Expression Vectors

1. IQSEC3. The shRNA AAV against mouse *Iqsec3* (GenBank accession number: NM_207617.1) was constructed by annealing, phosphorylating, and cloning oligonucleotides targeting mouse *Iqsec3* (5′-GAA CTG GTG GTA GGC ATC TAT GAG A-3′) into the *BamH*I and *EcoR*I sites of the pAAV-U6-GFP vector (Cell BioLabs, Inc.) AAVs encoding full-length shRNA-resistant rat *Iqsec3* WT and the E749A point mutant were generated by amplification of the full-length region by PCR and subsequent subcloning into the pAAV-T2A-tdTomato vector (a gift from Hailan Hu; [see (Li et al., 2013)]) at *Xba*I and *BamH*I sites. 2. Others. The DIO-human *SST* fragment (GenBank accession number: BC032625.1) was PCR-amplified and subcloned into the pAAV-hSYN-DIO-mCherry vector using the *Nhe*I site. The GW1-HA-ARF6 construct was previously described (Choi et al., 2006).

Antibodies

The following commercially available antibodies were used: goat polyclonal anti-EGFP (Rockland), mouse monoclonal anti-GAD67 (clone 1G10.2; Millipore), rabbit polyclonal anti-VGAT (Synaptic Systems), guinea pig polyclonal anti-VGLUT1 (Millipore), rabbit polyclonal anti-$GABA_AR\gamma2$ (Synaptic Systems), mouse monoclonal anti-parvalbumin (clone PARV-19; Swant), rat monoclonal anti-somatostatin (clone YC7; Millipore), rabbit polyclonal anti-CCK-8 (Immunostar), mouse monoclonal anti-Calretinin (clone 6B8.2; Millipore), rabbit polyclonal anti-SSTR2 (Thermo Fisher Scientific), rabbit polyclonal anti-SSTR4 (Thermo Fisher Scientific), mouse monoclonal anti-HA (clone 16B12; Biolegend), and rabbit polyclonal anti-MAP2 (Millipore). Rabbit polyclonal anti-IQSEC3 (JK079) (Um et al., 2016a) was previously described.

ARF6 Activation Assay

HE293T cells were transfected with HA-ARF6 alone or together with IQSEC3 WT or IQSEC3 E749A, and lysed 48 hours later. Cell extracts were subjected to an ARF6 activation assay according the manufacturer's instructions (Cell Biolabs). Cell extracts were immunoprecipitated with the provided GGA3 PBD agarose (recognizes GTP-bound ARF6), and ARF6 proteins were detected by immunoblot analysis using anti-HA antibodies.

Production of Recombinant Adeno-associated Viruses (AAVs)

Recombinant AAVs were packaged with pHelper and AAV1.0 (serotype 2/9) capsids for high efficiency. HEK293T cells were cotransfected with pHelper and pAAV1.0, together with pAAV-U6-EGFP alone (Control), pAAV-U6-shIQSEC3 (IQSEC3 KD), pAAV-IQSEC3 WT-2A-tdTomato (IQSEC3-WT), pAAV-IQSEC3 E749A-2A-tdTomato (IQSEC3-E749A), pAAV-hSYN-DIO-hSST-mCherry (DIO-hSST), or pAAV-hSYN-DIO-mCherry (Control). Transfected HEK293T cells were harvested 72–108 hours post transfection. After addition of 0.5 M EDTA to the media, cells were washed three times with phosphate-buffered saline (PBS) and collected by centrifugation. Cells were then resuspended in PBS and lysed by subjecting to four freeze-thaw cycles in an ethanol/dry ice bath (7 minutes each) and 37°C water bath (5 minutes). Lysates were centrifuged, and supernatants were collected and incubated with a solution containing 40% poly(ethylene glycol) (Sigma) and 2.5 M NaCl on ice for 1 hour and centrifuged at 2000 *rcf.* for 30 minutes. The pellets were resuspended in HEPES buffer (20 mM HEPES pH 8.0, 115 mM NaCl, 1.2 mM $CaCl_2$, 1.2 mM $MgCl_2$, 2.4 mM KH_2PO_4), mixed with chloroform, and centrifuged at 400 *rcf.* for 10 minutes. The supernatant was collected and concentrated using Amicon Ultra Centrifugal Filters (0.5 ml, 3K MWCO; Millipore). Viruses were assessed for infectious titer by RT-PCR, and used for infections at 1×10^{10}–10^{12} infectious units/μl.

Stereotaxic Surgery and Virus Injections

For stereotaxic delivery of recombinant AAVs, 9–week-old C57BL/6N mice were anesthetized by inhalation of isoflurane (3%–4%) or intraperitoneal injection of 2% 2,2,2-tribromoethanol (Sigma), dissolved in saline, and secured in a stereotaxic apparatus. Viral solutions were injected with a Hamilton syringe using a Nanoliter 2010 Injector (World Precision Instruments) at a flow rate of 100 nl/min (injected volume, 0.6 μl). The coordinates used for stereotaxic injections into hippocampal DG of mice were as follows: anteroposterior (AP), −2.1 mm; medial–lateral (ML), ± 1.2 mm; and dorsal–ventral (DV), 2.2 mm from bregma. Each injected mouse was returned to its home cage and used for scoring seizure-like behaviors, immunohistochemical analyses, or electrophysiological recordings after 2 weeks.

Seizure Behavior Scoring

9–week-old male C57BL/6N mice stereotactically injected with the indicated AAVs were administered KA (20 mg/kg; Sigma Cat. No. K0250), pilocarpine (290 mg/kg; Sigma Cat. No. P6503) or saline (control), and the resulting seizure behaviors were video-recorded for the next 2 hours. Seizure susceptibility was measured by rating seizures every 3 min on a scale of 0 to 5 as follows: no abnormal behavior (0), reduced motility and prostate position (1), partial clonus (2), generalized clonus including extremities (3), tonic-clonic seizure with rigid paw extension (4), and death (5).

EEG Recordings and Analyses

For EEG recordings, 6–week-old male C57BL/6N mice were anesthetized with isoflurane (3%–4%) and secured in a stereotaxic apparatus to ensure no limb-withdrawal response to a noxious foot pinch. After injection of the indicated concentrated AAVs into the hippocampal DG of experimental mice as described above, four additional holes were drilled in the skull without puncturing the meninges, and electrodes were carefully attached with prefabricated headmounts and secured with dental acrylic. Recording electrodes were placed in parietal lobe; AP −2.4 mm and ML ± 1.4 mm, and reference electrodes were placed in the occipital lobe. After a 2-week recovery period, mice connected to EEG/EMG three-channel monitoring SYSTEM (composed of preamplifier and a commutator for data acquisition system; Pinnacle Technology) with time-lock video recording, were transferred to an acrylic cage (25 × 25 × 45 cm). Each mouse was subjected to a 24-hour recording session for measuring spontaneous seizures and a 4-hour recording session for measuring KA-induced seizures. Data were recorded at a sampling rate of 400 Hz, with application of a 100-Hz loss-pass filter. Offline EEG analyses were performed manually in MATLAB (MathWorks) using EEGlab or LabChart 8.0 software (ADInstruments). For manual analyses of electrographic seizures, the following previously described criteria were used, with minor modifications (Baraban et al., 2009): grade I, basic background, no epileptiform spikes; grade II, mostly normal background, some high-voltage spikes; grade III, mostly abnormal background with low-frequency, high-voltage spiking; and grade IV, high-frequency, high-voltage, synchronized polyspike waves with amplitudes > 3-fold baseline. Only ictal seizures (grade III or grade IV) lasting longer than 3 s were included in the analysis. For automated quantification of interictal spikes, selected frequencies (0–60 Hz) were digitally filtered using low-pass filter in LabChart 8.0 software (ADInstruments) and amplitudes > 3-fold baseline discharges were automatically calculated using the native LabChart function.

Local Field Potential (LFP) Recordings and Analyses

9–week-old male mice were anaesthetized with 2% tribromoethanol (20 ml/kg, intraperitoneal injection) and placed on a stereotaxic device (David Kopf Instruments). AAVs expressing sh-Control or sh-IQSEC3 were injected bilaterally into the hippocampal DG

(AP, −1.94 mm; lateral, ± 1.0 mm; ventral, −2.0∼-2.2 mm) using a microsyringe pump (KDS Legato 130 Syringe Pump Control Box 788130; KDS Scientific). For hippocampal local field recordings, a Teflon-coated, stainless steel electrode was positioned unilaterally at the same coordinates as the virus injection site, and an epidural electrode for EEG recording was implanted in the contralateral parietal lobe (AP, −1.9 mm; lateral, +1.6 mm). As a reference electrode, an epidural screw was implanted into the occipital region of the skull. All electrodes were connected to a socket and fixed to the skull with dental acrylic resin. After 2 weeks of recovery from surgery, mice were placed in a clean cage and allowed to habituate. Seizures were induced in mice by intraperitoneal injection of KA (15 mg/kg in saline; Tocris, 0222) after performing LFP/EEG recordings for 10 minutes to measure baseline amplitude; animals were monitored for 240 minutes following injection. LFP/EEG signals were amplified (QP511 Quad AC Amplifier System, Grass Technologies) and digitized (sampling frequency, 500 Hz) using an Axon DigiData 1440A analog-digital converter (Molecular Devices). LFP/EEG signals were recorded simultaneously with video recordings for all groups. In LFP signals, epileptiform discharges (spikes and sharp waves), defined as high-amplitude (> 2 × baseline) and high-frequency (> 10 Hz) discharges that lasted for a minimum of 5 s, were quantified over 10-minute intervals using MATLAB. Spectrograms were obtained by filtering signals with a third-order Butterworth infinite impulse response (IIR), high-pass filter with a 10-Hz cutoff frequency prior to fast Fourier transformation, and were visualized using 0.5-Hz frequency resolution and 0.05 s time resolution. Normalized power spectral densities were summed for the three frequency ranges of hippocampal oscillations: theta (3–5 Hz), slow gamma (30–45 Hz), and fast gamma (55–80 Hz).

Immunohistochemistry and Imaging

11–week-old mice were anesthetized and immediately perfused, first with PBS for 3 minutes and then with 4% paraformaldehyde for 5 minutes. Brains were dissected out, fixed overnight in 4% paraformaldehyde, incubated overnight with 30% sucrose (in PBS), and then sliced into 30-μm-thick coronal sections using a vibratome (Model VT1200S; Leica Biosystems) or a cryotome (Model CM-3050-S; Leica Biosystems). Sections were permeabilized by incubating with 1% Triton X-100 in PBS containing 5% bovine serum albumen and 5% horse serum for 30 minutes. For immunostaining, sections were incubated for 8–12 hours at 4°C with primary antibodies diluted in the same blocking solution. The following primary antibodies were used: anti-IQSEC3 (JK079, 2 μg/ml), anti-$GABA_AR\gamma2$ (1:200), anti-GAD67 (1:100), anti-VGAT (1:300), anti-PV (1:500), anti-SST (1:50), anti-CCK-8 (1:300), anti-Calretinin (1:300), anti-SSTR2 (1:100), and anti-SSTR4 (1:2000). Sections were washed three times in PBS and incubated with appropriate Cy3- or fluorescein isothiocyanate (FITC)-conjugated secondary antibodies (Jackson ImmunoResearch) for 2 hours at room temperature. After three washes with PBS, sections were counterstained with DAPI (4',6-diamidino-2-phenylinodole) and mounted onto glass slides (Superfrost Plus; Fisher Scientific) with Vectashield mounting medium (H-1200; Vector Laboratories). Tiled Z stack images were acquired in standard mode with a laser-scanning confocal microscopy (Zeiss LSM800 with Airyscan module) equipped with 40x or 63x objective (0.156 μm/pixel; X-Y dimension 1024 × 1024) and Zen2.6 Software (Zeiss). Z stacks were configured using Acquisition dimensions, and 8–10 slices with a 2-μm interval setting. For quantifications, MetaMorph Software (Molecular Devices) was used as follows: region of interest (ROI) was manually chosen, calibrated (using the Length Calibration function), and thresholded (using the Threshold function; 100 minimum and 255 maximum) to remove background signals. Synaptic puncta in the size range 0.1∼10 μm^2 were counted using the Histogram function.

Electrophysiology

Transverse hippocampal slices (300 μm) were prepared from 10–12-week-old male mice, as previously described (Um et al., 2016b). Mice were anesthetized with isoflurane and decapitated. The brains were rapidly removed and placed in ice-cold, oxygenated (95% O_2 and 5% CO_2) low-Ca^{2+}/high-Mg^{2+} solution containing the following: 3.3 mM KCl, 1.3 mM NaH_2PO_4, 26 mM $NaHCO_3$, 11 mM D-glucose, 0.5 mM $CaCl_2$, 10 mM $MgCl_2$, and 211 mM sucrose. Hippocampal slices were cut with a VT1000s vibratome (Leica) and transferred for recovery to a holding chamber containing oxygenated artificial cerebrospinal fluid (aCSF) consisting of the following: 124 mM NaCl, 3.3 mM KCl, 1.3 mM NaH_2PO_4, 26 mM $NaHCO_3$, 11 mM D-glucose, 2.5 mM $CaCl_2$, and 1.5 mM $MgCl_2$. Slices were stored at 30°C for at least 60 minutes, and all slices were used within 5 hours of preparation. After recovery, slices were placed in the recording chamber, where they were perfused continuously with normal aCSF bubbled with 95% O_2 and 5% CO_2. All experiments were performed at 28–29°C. Whole-cell recordings of miniature postsynaptic currents were carried out on DG granule neurons, with voltage clamped at −70 mV. For mIPSC recordings, glass pipettes (3-5 MΩ) were filled with an internal solution containing the following: 145 mM CsCl, 5 mM NaCl, 10 mM HEPES, 10 mM EGTA, 4 mM Mg-ATP, and 0.3 mM Na-GTP. The osmolarity of the internal solution was 290–300 mOsm and the pH was 7.3 (adjusted with CsOH); 1 μM TTX, 10 μM CNQX and 50 μM AP-5 were added to block Na^+ currents, AMPARs and NMDARs, respectively. For mEPSC recordings, 1 μM TTX and 50 μM picrotoxin were added to block Na^+ currents and $GABA_A$ receptors, respectively. Evoked inhibitory synaptic responses were induced in the DG by placing a concentric bipolar electrode (FHC) at the DG molecular layer for dendritic inhibition. For evoked inhibitory postsynaptic current recordings, glass pipettes were filled with an internal solution containing the following: 130 mM Cs-methanesulfonate, 5 mM TEA-Cl, 8 mM NaCl, 0.5 mM EGTA, 10 mM HEPES, 4 mM Mg-ATP, 0.4 mM Na-GTP, 2.5 mM QX-314, and 10 mM disodium phosphocreatine. The osmolarity of the internal solution was 290–300 mOsm and the pH was 7.3 (adjusted with CsOH). If access resistance changed more than 20% or exceeded 30 MΩ, data were discarded.

Neuron Culture, Imaging, and Quantification

Cultured hippocampal rat neurons were prepared from E18 rat embryos, as previously described (Ko et al., 2003, 2011), cultured on coverslips coated with poly-D-lysine (Sigma), and grown in Neurobasal medium supplemented with B-27 (Thermo Fisher), 0.5% FBS (WELGENE), 0.5 mM GlutaMAX (Thermo Fisher), and sodium pyruvate (Thermo Fisher). The rat embryonic cortices were dissected and isolated in Hank's Balanced Salt Solution (HBSS) containing 10 mM HEPES (pH 7.4), and incubated in HBSS containing 14 U/ml papain (Worthington) and 100 μg/μl DNase I for 15 minutes at 37°C. After washing, tissues were dissociated by pipetting, plated on poly-D-lysine and laminin-coated coverslips (Corning) in Neurobasal media (Invitrogen) supplemented with B27 (Invitrogen), Glutamax (Invitrogen), FBS (2.5%, Invitrogen), and penicillin/streptomycin (0.5x, Invitrogen). After 1 week, half of the medium was replaced with FBS-free medium. For immunocytochemistry, cultured neurons were fixed with 4% paraformaldehyde/4% sucrose, permeabilized with 0.2% Triton X-100 in PBS, immunostained with the indicated primary antibodies, and detected with the indicated Cy3- and fluorescein isothiocyanate (FITC)-conjugated secondary antibodies (Jackson ImmunoResearch). Images were acquired using a confocal microscope (LSM780, Carl Zeiss) with a 63x objective lens; all image settings were kept constant. Z stack images were converted to maximal projection and analyzed to obtain the size, intensity, and density of puncta immunoreactivities derived from marker proteins. Quantification was performed in a blinded manner using MetaMorph software (Molecular Devices).

QUANTIFICATION AND STATISTICAL ANALYSIS

All data are expressed as means ± SEM. All experiments were repeated using at least three independent cultures, and data were statistically evaluated using a Mann-Whitney *U* test, analysis of variance (ANOVA) followed by Kruskal-Wallis test followed by Dunn's pairwise post hoc test. Prism7.0 (GraphPad Software) was used for analysis of data and preparation of bar graphs. *P*-values < 0.05 were considered statistically significant (individual *p-value*s are presented in figure legends).

DATA AND CODE AVAILABILITY

This study did not generate datasets.